Ultrasonic sectorial inspection in the presence of temperature gradients

Mateus Yamada Müller[1], Tatiana de Almeida Prado[1], Thiago Estrela Kalid[1]
Thiago Alberto Rigo Passarin[1] and Daniel Rodrigues Pipa[1]
1 Federal University of Technology – Parana (UTFPR), Brazil,
passarin@professores.utfpr.edu.br.

Abstract

Ultrasonic nondestructive testing is a precise tool for equipment inspections. Among the usual methods, sectorial scanning stands out within contact-based techniques, as it provides broad angular sweeps without the need to physically steer the transducer, and the configuration of the beams hinges on the geometry of the tested objects. However, in high-temperature scenarios (e.g., oil treatment vessels), thermal gradients along the propagation path result in inaccurate sizing of discontinuities, given that the presence of such gradients is responsible for variations in the velocities and distortions of the ultrasonic beams. This paper proposes a method to compensate for these distortions during the sectorial inspection. Optimal linear approximation parameters are determined offline from a controlled Full Matrix Capture (FMC) test, in which the setup consists of a phased array transducer, a high-temperature resistant wedge and an aluminium test block with flaws at known positions. The positions of the flaws are measured on the Total Focusing Method (TFM) reconstructions, and the parametric velocity models for specific instants of heating time are estimated through the minimization of a cost function. Then, focal laws are calculated from the parameters using the ray tracing technique and stored in a text file to be interpreted by the instruments as a native focal law. An online test is proposed for validating the method at the controlled temperature of $70^{o}C$. The results show that the positions of the flaws, and the distance between them in the S-scan image, present improved accuracy (with errors reduced by approximately 64%) when the proposed correction is applied.

1. Introduction

The oil and gas industry relies on equipment operating at high temperatures for long periods. On an industrial scale, ultrasound non-destructive testing is utilized as a method for predictive inspections, given its capacity of precise flaw detection. However, the distortions on the ultrasonic beams make high-temperature inspections difficult, as the anisotropy imposed by temperature variations may cause inaccurate sizing and positioning of flaws. In order to reduce these inaccuracies, it is necessary to adopt specific focal laws, calculated based on heat propagation models.

 https://doi.org/10.58286/28122

High temperatures put ultrasonic probes at risk as they tend not to resist them, with manufacturers recommending direct contact operating temperatures up to a maximum of 60^oC [1]. This issue often results in the need to shut down oil treatment plants to carry out evaluations safely, with the outcome of ceasing production during possibly prolonged periods [2]. Therefore, the potential to monitor discontinuities online and at high temperatures is significant to decision-making in the event of irregularities, potentially avoiding unnecessary interruptions [3].

This paper proposes an approach based on sectorial scanning allied with the adoption of optimal parameters, that aims to compensate for the distortions of the beams, hence, improving the accuracy of the image reconstructions. The work is organized as follows. Section 2 presents the test setup and methodologies chosen to yield the optimal parameters, also the calculation of the focal laws based on the ray tracing technique from the parameters. In Section 3, the validation of the proposed method is presented through experimental results. Finally, Section 4 presents the discussions of the results and conclusions.

2. Proposed Method

Inspections of test blocks under high temperature require analysis of the influence of the thermal gradients in the propagation of the ultrasonic beams. To simplify the problem, a linear temperature gradient was considered, responsible for variations in the velocity and distortions of the beams that go through it. This gradient is dynamic for a short period, tending to stabilize after some minutes.

Velocity parameters were yielded through linear approximation of the data from a set of laboratory-controlled tests. In these tests, the following setup was implemented: Olympus 5L64-A32 phased array transducer, Olympus SA32C-ULT-N55S-IHC high-temperature wedge, M2M Panther ultrasound system along with its dedicated software Acquire, a thermostatic bath and an aluminum test block with two grooves at known positions, highlighted by Figure 1a. A structure, shown in Figure 1b, maintained the ensemble steady. With the test block under constant temperature, every thirty seconds during a sixty minutes interval, FMC [4] acquisitions were performed to monitor the evolution of the gradient in the wedge. This technique provides wide post-processing, which is essential to the offline calculations of the optimal parameters.

Assuming a linear dependency of the velocity in the temperature [5] and considering that the temperature varies linearly along the top and the bottom of the wedge, an approximation of the velocity $v(z)$ as a function of the height z was formulated

$$v(z) = v_0 + \frac{v_1 + v_0}{z_1 + z_0} z, \tag{1}$$

where v_0 is the sound propagation velocity at the interface between the wedge and the test block, and v_1 is the sound propagation velocity at the top of the wedge.

The optimal parameters v_0, v_1 and c_s (shear propagation velocity in the test block) were determined through the minimization of the cost function

$$\phi(x_1, z_1, z_2) = (x_1 - x_{real})^2 + (z_1 - z_{real})^2 + [(z_1 - z_2) - \Delta z_{real}]^2, \tag{2}$$

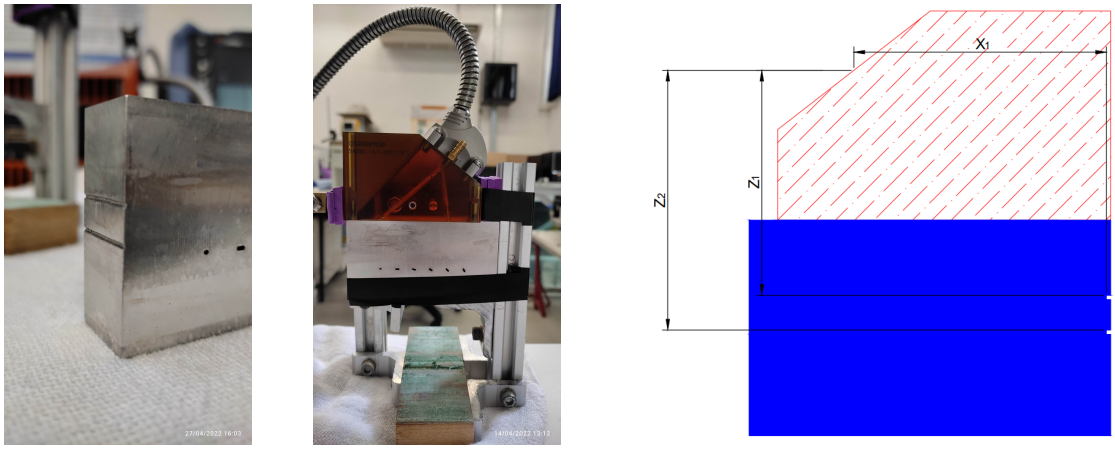

(a) (b) (c)

Figure 1: a) Aluminum test block. b) Structure to keep the equipments steady. c) Convention of the coordinates used in the sizing of the flaws.

which synthesizes the three criteria of how much the beam was distorted: the horizontal position of the flaw in the test block (x_1), the heights of the flaws (z_1 and z_2) and the height difference between them, illustrated by the Figure 1c. x_{real}, z_{real} and Δz_{real} represent measurements at room temperature. For the particular case of Figure 1a, the values are x_{real} = 66.38 mm, z_{real} = 52.50 mm and Δz_{real} = 8.00 mm, all considering the center element of the transducer as the reference.

From the defined search interval (v_0 and v_1 from 2360 to 2460 m/s with a 10 m/s step, and for c_s from 3085 to 3135 m/s with a 5 m/s step), the images were reconstructed by the Total Focusing Method (TFM) algorithm [4] using all the possible combinations of the three parameters. For each attempt, x_1, z_1 and z_2 were measured in the result of the reconstruction, and then substituted on the Eq.(2). The chosen optimal parameters were the ones that provided the lowest value of the cost function Φ among the possible combinations.

The velocity c_s was estimated for the last instant of time, considering that the temperature was stabilized. It was detected that the optimal point occurs for a value of c_s=3115 m/s. Assuming c_s constant during the whole inspection, a new search was done to calculate the optimal values for v_0 and v_1. This last step was repeated for each instant of time from 0 to 60 minutes. The results are shown in Figure 2.

2.1 Focal laws

From the parameters presented in this section, the necessary time delay in the excitation of each element was calculated, enabling the desired wavefront generation [6]. In order to generate a plane wave at a specific refracted angle θ, a firing angle search process is executed for each element of the active aperture.

The delays are calculated so that the difference between two consecutive entrance time instants (when the wavefront reaches the entrance point in the test block) is

$$d_n = \frac{(x_n - x_{n-1})\,\mathrm{sen}(\tilde{\theta})}{c}, \tag{3}$$

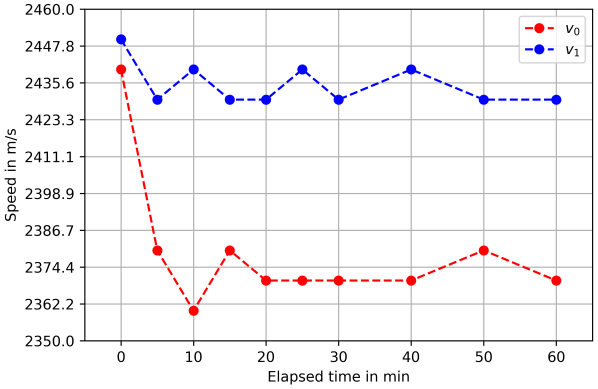

Figure 2: Velocities obtained, for each instant of time, from the optimal shear velocity value on the test block.

where x_{n-1} and x_n are the horizontal coordinates of consecutive entrance points, $\tilde{\theta}$ is the non-refracted incidence angle at the entrance point (the Snell's law gives its relation with θ) and c is the sound propagation velocity in the wedge. Then, specific focal laws are calculated for each temperature condition and written in a LAW text file format, as expected by TomoView software. This file type was chosen because the focal law tool, Advanced Calculator, cannot compute laws with different propagation velocities in the wedge.

3. Results

The proposed method was validated through one online multigroup sectorial scan (with an active aperture of 16 elements starting from the 32nd element) utilizing the Omniscan/TomoView set. For each group, a distinctive LAW file was imported (Table 1) to validate the correction in the sizing by the optimal parameters. These files were calculated as presented in subsection 2.1. Given that the validation needed to be performed at a high temperature, the aluminum test block was heated in the thermostatic bath until 70^oC. The data was acquired 60 minutes after the wedge came in contact with the test block.

Table 1: Configuration of the velocities for each high-temperature inspection group.

Group	c_s **[m/s]**	v_0 **[m/s]**	v_1 **[m/s]**
Corrected high-temperature	3115	2370	2430
Uniform 2370 high-temperature	3115	2370	2370
Uniform 2366 high-temperature	3115	2366	2366
Uniform 2455 high-temperature	3115	2455	2455

The positions of the grooves, Figure 1a, were measured from the pair of maximum echoes in the files of each inspection. This method is known as diffraction technique [7], where the position identification of the pixel with the highest amplitude in the S-scan image is attained by searching the peak with the highest amplitude in the A-scans. The Table 2 and the Figure 3 present the values of relative height between the flaws, absolute positions of each flaw and some relevant S-scan images.

Table 2: Position of the flaws and distance between them, considering the interface amid wedge and aluminum as the reference.

Sizing [mm]	Absolute position		Distance between flaws
	Flaw 1	Flaw 2	
	z	z	z
True known values	18.64	26.54	7.90
Corrected high temperature	18.72	27.23	8.51
Uniform 2370 high temperature	17.13	26.19	9.06
Uniform 2366 high temperature	16.37	25.39	9.02
Uniform 2455 high temperature	18.97	28.55	9.58

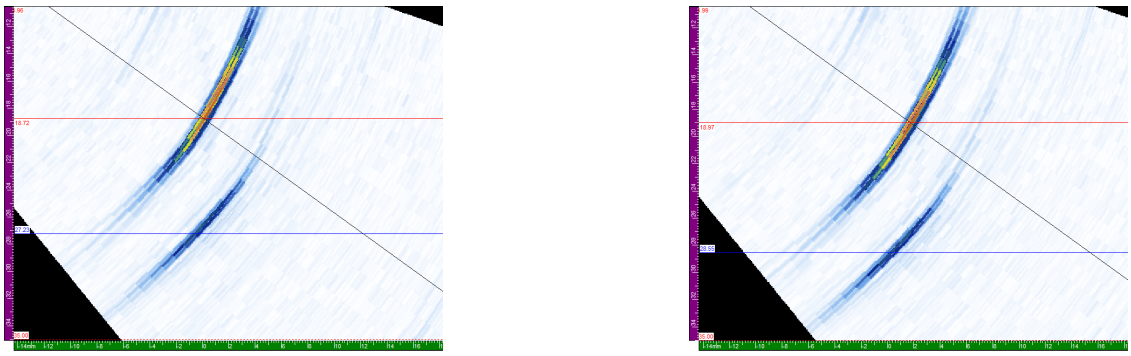

(a) (b)

Figure 3: S-scan images from two critical cases of the validation: one represents the correction of the distortions imposed by the gradient, and the other is the result of delay laws without any form of compensation. The black line indicates the 55^o angle of the sectorial scan. The red and blue lines mark the vertical positions of the pixels with the highest amplitude for each groove of the aluminum test block (Figure 1a). (a) Corrected high temperature. (b) Uniform 2455 high temperature.

As the actual positions of the flaws on the test block are known, these values can be compared with those estimated using the synthesized LAW files. Thus, the real measurements at room temperature were adopted as the reference. The availability of these measurements avoids the need to perform a reference inspection at room temperature, which would also require exclusive optimal parameters to calculate the delays.

For the groups "Uniform 2370 and 2366 high temperature" (respectively, optimal v_0 and the sound propagation velocity in the wedge experimentally yielded for 70^oC), the velocities were chosen considering the heated wedge, but without the gradient yet. In the third group, "Uniform 2455 high temperature" (without gradient compensation), it was considered an approximated velocity for the sound propagation at room temperature. When the optimal parameters were adopted, the error in the distance between the flaws was significantly reduced compared to the previous three groups. Likely because the cost function minimization calibrates the calculation of the delays based on the real propagation paths. The results of the relative errors between the high-temperature measurements and the reference are shown in Table 3.

Table 3: Relative errors between the reference and the multigroup inspection at 70^oC.

Relative error [%]	Position error		Distance error
	Flaw 1	Flaw 2	
Corrected high temperature	0.43	2.60	7.72
Uniform 2370 high temperature	8.10	1.32	14.68
Uniform 2366 high temperature	12.18	4.33	14.18
Uniform 2455 high temperature	1.77	7.57	21.27

4. Conclusions

In this paper, a method to correct measurements of flaws at high-temperature ultrasonic sectorial inspections was proposed. The results demonstrate the applicability of the proposed method, presenting that the adoption of a linear thermal gradient model and optimal parameters enable a reconstruction of S-scan images with reduced distortions and, hence, better accuracy in the positioning of flaws.

Acknowledgments

The authors acknowledge the financial support from PETROBRAS/CENPES through project AUSPEX, CNPq through grant 316234/2021-4, and CAPES - Finance Code 001. The authors also would like to thank UTFPR, Fundação Araucária, FINEP and NUEM.

References

1. J. S. Slongo, J. Gund, T. A. R. Passarin, D. R. Pipa, J. E. Ramos, L. V. Arruda, and F. Neves. "Effects of Thermal Gradients in High-Temperature Ultrasonic Non-Destructive Tests". In: *Sensors* 22.7, 2022.
2. F. B. Cegla, P. Cawley, J. Allin, and J. Davies. "High-Temperature (> 500^oC) Wall Thickness Monitoringh Using Dry-Coupled Ultrasonic Waveguide Transducers". In: *IEEE Transactions on Ultrasonics, Ferroelectrics, and Frequency Control* 58.1, pp. 156–167, 2011.
3. S. P. Kelly, D. Babcock, I. Atkinson, C. Gregory, and K. J. Kirk. "On-line Ultrasonic Inspection at Elevated Temperatures". In: *2007 IEEE Ultrasonic Symposium Proceedings*. New York, NY, pp. 904–908, 2007.
4. C. Holmes, B. W. Drinkwater, and P. D. Wilcox. "Post-processing of the full matrix of ultrasonic transmit-receive array data for non-destructive evaluation". In: *NDT and E International* 38.8, pp. 701–711, 2005.
5. M. Marvasti, J. Bond, M. Mathenson, and A. N. Sinclair. "Phased array inspection at elevated temperatures: Effects of ultrasonic beam skew". In: *Insight* 56.5, pp. 256–263, 2014.
6. N. Dubé, M.D.C. Moles, C.R. Bird, P. Herzog, T. Armitt, P. Ciorau, R. Roberts, and M. Davis. *Introduction to Phased Array Ultrasonic Technology Applications*. Olympus, 2017.
7. F. Jacques, F. Moreau, and E. Ginzel. "Ultrasonic backscatter sizing using phased array - developments in tip diffraction flaw sizing". In: *Insight* 45.11, pp. 724–728, 2003.